Mol Cell Proteomics Papers in Press. Published on October 29, 2018 as Manuscript RA118.001102

Common metabolic pathways implicated in resistance to chemotherapy point to a key mitochondrial role in breast cancer

Etna Abad[1], Yoelsis García-Mayea[1], Cristina Mir[1], David Sebastian[2,3,4], Antonio Zorzano[2,3,4], David Potesil[5], Zbynek Zdrahal[5,6], Alex Lyakhovich[1]*, Matilde E. Lleonart[1,7,*]

[1]Biomedical Research in Cancer Stem Cell Group, Pathology Department, Vall d'Hebron Hospital, 08035, Passeig Vall d´Hebron 119-129, 08035 Barcelona. Barcelona, Spain.

[2]Institute for Research in Biomedicine (IRB Barcelona), The Barcelona Institute of Science and Technology, Barcelona 08028, [3]Departament de Bioquímica i Biomedicina Molecular, Universitat de Barcelona, c/ Baldiri Reixac, 10-12, Barcelona 08028, Spain; [4]CIBER de Diabetes y Enfermedades Metabólicas Asociadas (CIBERDEM), Instituto de Salud Carlos III, Madrid 28029, Spain;

[5]CEITEC - Central European Institute of Technology, Masaryk University, Brno, Czech Republic and [6]National Centre for Biomolecular Research, Faculty of Science, Masaryk University, Kamenice 5, 62500 Brno, Czech Republic.

[7]Spanish Biomedical Research Network Centre in Oncology, CIBERONC, Barcelona, Spain

Running title: OMICS approaches revealed linezolid as anticancer drug

The authors declare no potential conflicts of interest.

* Corresponding: alex.lyakhovich@vhir.org; matilde.lleonart@vhir.org

Abbreviations page

ATP adenosine triphosphate

BCA assay the bicinchoninic acid assay to determine concentration of protein

CSC cancer stem cells

ROS reactive oxygen species

OXPHOS oxidative phosphorylation

Mitoribosomes mitochondrial ribosomes

TNBC triple-negative breast cancer

TNBT triple negative breast tumour

MDF mitochondrial dysfunction

Rho^0 cells depleted of mitochondrial DNA

$\Delta\Psi m$ mitochondrial membrane potential

TCA tricarboxylic acid

OCR oxygen consumption rate

HCQ hydroxychloroquine

Summary:

Cancer cells are known to reprogram their metabolism to adapt to adverse conditions dictated by tumour growth and microenvironment. A subtype of cancer cells with stem-like properties, known as cancer stem cells (CSC), is thought to be responsible for tumour recurrence. In this study, we demonstrated that CSC and chemoresistant cells derived from triple negative breast cancer cells display an enrichment of up- and down-regulated proteins from metabolic pathways that suggests their dependence on mitochondria for survival. Here, we selected antibiotics, in particular – linezolid, inhibiting translation of mitoribosomes and inducing mitochondrial dysfunction. We provided the first *in vivo* evidence demonstrating that linezolid suppressed tumour growth rate, accompanied by increased autophagy. In addition, our results revealed that bactericidal antibiotics used in combination with autophagy blocker decrease tumour growth. This study puts mitochondria in a spotlight for cancer therapy and places antibiotics as effective agents for eliminating CSC and resistant cells.

Introduction:

Cancer cells are known to reprogram their metabolism in order to adapt to their high proliferation rate and specific requirements, switching from oxidative phosphorylation (OXPHOS) to aerobic glycolysis, thus allowing the cells to rapidly produce adenosine triphosphate and building blocks like ribonucleotides and amino acids while generating lactate (1). These phenomena, originally described by Otto Warburg, presented a compelling demonstration that most cancer cells exploit this strategy because of their constant need for adaptation to microenvironment as well as maintaining rapid growth (2, 3). We previously described that the Warburg effect initially discovered in cancer cells can also be a characteristic of cells with stemness properties (4). Recent evidence regarding CSC, a subtype of cancer cells with stem-like properties, suggests that it is this cell subpopulation that is responsible for cancer metastases as their isolation and xenotransplantation in animal models provoke metastasis (5–7). This suggests that effective anticancer therapy may require targeting and eliminating a subset of tumour preserving CSC and resistant cells, from a continuous production of progeny.

Although much controversy remains about the validity of CSC and their connection to chemoresistant tumours, it seems likely that both CSC and chemoresistant cells may share common qualities (8). For example, residual breast cancer cells, after either, hormonal or chemo-therapy are enriched in CSC markers (9). In turn, biopsies from the most aggressive breast cancer subtype, known as chemoresistant triple-negative breast cancers (TNBC), showed an increased expression of genes associated with CSC (10). Although efficient anti-cancer therapy seems to require targeting CSC within a given patient, most of the

approaches available so far are limited by their plasticity, co-expression of non–CSC markers, and variations between experimental models (11). In addition, intra-tumour heterogeneity allows coexisting of cancer cells that rely on both glycolysis and OXPHOS within the same tumour mass, indicating a survival adaptation to overcome chemoresistance (11, 12). Regardless of the precise mechanisms, these different metabolic signatures suggest mitochondria involvement in the cancer cell energy production which may represent a potential target for anticancer therapy(13, 14).

On the other hand, the accumulated evidence indicates that several bactericidal antibiotics may effectively induce mitochondrial dysfunction (MDF), suppress the growth of cancer cells and, perhaps, tumours (15–17). Thus, treatment of cancer with specific antibiotics may appear as a novel anticancer strategy. Moreover, in order to maintain metabolic homeostasis and cell viability, cancer cells activate catabolic processes, including autophagy, which helps them not only to survive and proliferate but also to achieve a high resistance to microenvironmental insults. In turn, autophagy can be induced by many factors, including antibiotics, causing the elimination of dysfunctional mitochondria and providing additional survival pathway for cancer growth and metastatic relapse (18). In this sense, previous work from our group suggests that simultaneous treatment with specific antibiotics and autophagy blockers may hold a great therapeutic value (19).

In this study, functional analysis of TNBC cells and corresponding CSC and chemoresistant cancer cells revealed distinct pathway enrichment of up- and down-regulated proteins and upregulation of metabolites and suggested a direct link to mitochondria. To that end, we have studied the effects of antibiotics on mitochondrial functions and validated several of them in *in vitro* and *in vivo*

models of TNBC. In parallel, we demonstrated several mechanisms by which antibiotics suppress tumorigenic properties of CSC and chemoresistant cancer cells. Finally, we propose that antibiotics serving as MDF-inducers can suppress cancer cell proliferation and decrease tumour growth. In combination with autophagy blockers, such drugs can be repurposed as part of the multitarget anticancer therapy.

Experimental procedures:

Chemicals and antibiotics – A panel of the following antibiotics were tested: Hygromycin B (Invivogen, ant-hm-1), Chloramphenicol (Sigma Aldrich, C0378), Kanamycin (Thermo Fisher, 11815024) Ampicillin (Sigma, A9518), Tetracyclin (Sigma-Aldrich, T7660), Telithromycin (MedChem Express, HY-A0062), Capreomycin Sulfate (Selleckchem, S-4234), Viomycin (Tocris Bioscience, 3787), Linezolid (Sigma, PZ0014) and HCQ (Sigma, H0915). Cisplatin (cis-Diammineplatinum (II) dichloride, 479306) was purchased from Sigma-Aldrich. Cyclophosphamide and doxorubicin were obtained from Vall d'Hebron Hospital's pharmacy (Barcelona, Spain). A mixture of ROS scavengers (all from Thermo Fisher) were used: sodium pyruvate (10 mM final), mannitol (20 mM final), N-acetylcysteine (2 mM final).

Cell lines and tumoursphere formation – MDA-MB-231 commercial cell line (further called Parental or 231-Par) was purchased from ATCC. Cells were cultured in Dulbecco's modified Eagle's medium/F12 and supplemented with 10% FBS, 1% Pen-Strep, 1% Sodium Pyruvate and 1% L-glutamine. Chemoresistant cell lines (231-R) were established with continuous treatment for 6 months with anticancer therapeutic agents, such as cisplatin (231-Rcispl), doxorubicin (231-Rdox) and cyclophosphamide (231-Rcyclo). To obtain CSC

(231-CSC), we followed our previously published approach (20). In brief, a single cell suspension of parental cells was prepared using enzymatic disaggregation and cells were plated at a density of 10.000 cells per ml in Cancer Stem Cell medium (PromoCell, C-28070) in Poly-HEMA (Santa Cruz Biotechnology, sc-253284) coated plates. The cells were later verified using known stem cell markers. Rho^0 cells were obtained from 231-Par and 231-Rcyclo cells by treatment for 6-8 weeks with low dosages (50 ng/ml) of Ethidium Bromide (EtBr). Rho^0 resultant cell lines were maintained in complete DMEM/F12 containing 1 mM uridine. mtDNA depletion was tested by semi-quantitative PCR and Western blotting, mitochondrial membrane potential loss and disruption of the OCR profile (SeaHorse). Experiments related to measurement of respiration, ATP levels and activities of mitochondrial complexes were performed in the media containing no antibiotics.

Samples preparation and LC-MS/MS analyses – Samples were processed by filter-aided sample preparation (FASP) method. They were lysed with SDT buffer (4% SDS, 100 mM DTT, 100 mM Tris, pH 7.6) for 15 min at 95 ºC. Then, samples were mixed with 8M UA buffer (8M urea in 100 mM Tris-HCl, pH 8.5), loaded onto the Microcon device, with MWCO 30 kDa (Merck Millipore) and centrifuged at 7,000× g (the next centrifugation steps done at 14,000× g) for 30 min at 20°C. The retained proteins were washed with 200 µL UA buffer. The final protein concentrates kept in the Microcon device were mixed with 100 µL of UA buffer containing 50 mM iodoacetamide and incubated in the dark for 20 min. After the next centrifugation step, the samples were washed three times with 100 µL UA buffer and three times with 100 µL of 50 mM $NaHCO_3$. Trypsin (sequencing grade, Promega) was added onto the filter and the mixture was incubated for 18

h at 37°C. The tryptic peptides were finally eluted by centrifugation followed by two additional elutions with 50 µL of 50mM $NaHCO_3$. Resulting peptides were extracted into LC-MS vials by 2.5% formic acid (FA) in 50% acetonitrile (ACN) and 100% ACN with addition of polyethylene glycol (20,000; final concentration 0.001%) and concentrated in a SpeedVac concentrator (Thermo Fisher Scientific).

LC-MS/MS analyses of peptide mixtures were done using RSLCnano system connected to Orbitrap Elite hybrid spectrometer (Thermo Fisher Scientific). Prior to LC separation, tryptic digests were online concentrated and desalted using trapping column (100 µm × 30 mm) filled with 3.5-µm X-Bridge BEH 130 C18 sorbent (Waters). After washing of trapping column with 0.1% formic acid (FA), the peptides were eluted (flow 300 nl/min) from the trapping column onto an analytical column (Acclaim Pepmap100 C18, 3 µm particles, 75 µm × 500 mm; Thermo Fisher Scientific) by 100 min nonlinear gradient program (1-56% of mobile phase B; mobile phase A: 0.1% FA in water; mobile phase B: 0.1% FA in 80% ACN). Equilibration of the trapping column and the column was done prior to sample injection to sample loop. The analytical column outlet was directly connected to the Digital PicoView 550 (New Objective) ion source with PicoTip emitter SilicaTip (New Objective; FS360-20-15-N-20-C12). ABIRD (Active Background Ion Reduction Device) was installed.

MS data were acquired in a data-dependent strategy selecting up to top 10 precursors based on precursor abundance in the survey scan (350-2000 m/z). The resolution of the survey scan was 60 000 (400 m/z) with a target value of 1×10^6 ions, one microscan and maximum injection time of 200 ms. HCD MS/MS spectra were acquired with a target value of 50 000 and resolution of 15 000 (400

m/z). The maximum injection time for MS/MS was 500 ms. Dynamic exclusion was enabled for 45 s after one MS/MS spectra acquisition and early expiration was disabled. The isolation window for MS/MS fragmentation was set to 2 m/z.

Experimental design and statistical rationale – Pilot experiments for the estimation of tolerable dose of antibiotic have been performed with 3 animals in group. Experiments with linezolid alone or in combination with autophagy blocker have been performed two times (n=5 in each group). According to the rules of Ethical Committee (VHIR, Barcelona), animals were sacrificed when tumour volumes exceeded 2 cm^3. For the purpose of all experiments, individual biological replicates (from 3 to 5) comprised pooled preparations of total cell extracts isolated from MDA-MB-231 parental, cancer stem, or resistant cells to be used for tandem mass tag labeling in order to generate our primary inventory and to facilitate comparative and quantitative proteomic analyses. Proteins were identified as being differentially accumulated between extracts if they experienced a fold change of ≥ -1.5 or ≤ 1.5; $P < 0.05$. Immunoblotting of candidate proteins was performed (n = 2-4) for the 20 upregulated and 12 downregulated proteins in order to validate quantitative proteomics data. Further details of experimental design including the number of animals are provided in corresponding sections. The analysis of the mass spectrometric RAW data files was carried out using the Proteome Discoverer software (Thermo Fisher Scientific; version 1.4) with in-house Mascot (Matrixscience, London, UK; version 2.6) and Sequest search engines utilisation. MS/MS ion searches were done at first against the modified cRAP database (based on http://www.thegpm.org/crap/; 111 sequences in total) containing protein contaminants like keratin, trypsin etc. MS/MS spectra assigned by Mascot search engine to any cRAP protein peptide

with Mascot ion score >30 were excluded from the next database searches. Final database searches were done against UniProtKB proteome database for Homo sapiens (taxonomy ID 9606; canonical database version downloaded from ftp://ftp.uniprot.org/pub/databases/uniprot/current_release/knowledgebase/reference_proteomes/Eukaryota/UP000005640_9606.fasta.gz, database version 2017-07, number of proteins 20,975). Mass tolerance for peptides and MS/MS fragments were 10 ppm and 0.05 Da, respectively. Oxidation of methionine, deamidation (N, Q) and acetylation (protein N-terminus) as optional modification, carbamidomethylation (C) as fixed modification, trypsin specificity (C-terminal to K and R, except P follows) and one enzyme miss cleavage were set for all searches. Percolator was used for post-processing of the search results. Peptides with q-value <0.01, rank 1 and with at least 6 amino acids were considered only. Proteins matching the same set of peptides were reported as protein groups. Protein groups were reported only if they had at least one unique peptide. Label-free quantification using protein area calculation in Proteome Discoverer was used ("top 3 protein quantification"). Protein group reports for all individual samples (see Supplementary Table S1) were combined into a single supergroup (SG) table. Protein abundance ratios were calculated using SG areas. Median log2 transformed ratio was subtracted from all log2 transformed ratios to adjust them on different sample loading. Top altered proteins were validated by Western blot procedure (data not shown). The mass spectrometry proteomics data have been deposited to the ProteomeXchange Consortium via the PRIDE partner repository.

Tumour samples and preparation – TNBT samples and data from patients included in this study were provided by the Tumor Bank of Vall d'Hebron

University Hospital Biobank (PT13/0010/0021), integrated in the Spanish National Biobanks Network and Xarxa de Bancs de Tumors de Catalunya (XBTC), and they were processed following standard operating procedures with the appropriate approval of the Ethical and Scientific Committees. Tissues were homogenized on ice, lysed with RIPA buffer (0.5 M Tris-HCl, pH 7.4, 1.5 M NaCl, 2.5% deoxycholic acid, 10% NP-40, 10 mM EDTA, 2% SDS), sonicated on ice and centrifuged. Samples were normalized to total protein concentrations by either measuring the amount of proteins or quantifying the band intensities in coomassie-stained gel followed by Western blotting procedure.

NMR metabolite profiling – Approximately 5 mln cells were collected by trypsinization, span at 300g, washed in PBS, resuspended and kept frozen in 200uL of PBS until further use. When all samples were collected, resuspended cells were lyophilized overnight. 600 uL of D_2O were added to reconstitute lyophilized cells followed by transferring to a 5mm NMR tube. Cell pellet was extracted by adding 660 uL of a cold mixture of dichloromethane/methanol (2:1 v/v). The resulting suspension was vortexed and bath-sonicated for 1 min. We subsequently added 140 µL of cold water, vortex samples again and organic and aqueous layers were allowed to equilibrate for 10 min at room temperature. Cell lysates were centrifuged (15,000 rpm, 15 min at 4 °C), and 320uL of aqueous phase (upper layer) was collected for drying under a stream of nitrogen. Cell pellet was resuspended in 600uL of D2O and transferred to a 5mm NMR tube. 1H-NMR spectra were recorded at 300K on a Bruker Avance III 500 spectrometer coupling a X-PRESS sample changer operating at a proton frequency of 500 MHz. One-dimensional 1H pulse experiments were carried out using the nuclear Overhauser effect spectroscopy (NOESY)-presaturation sequence to suppress

the residual water peak at around 4.7 ppm. The relaxation delay between scans was set to 5 s. Mixing time was 100 ms and spectral width was 12.000 Hz (20 ppm), and a total of 32 transients for cell media and 256 transients for cell pellet were collected into 32k and 256k data points for each spectrum. The acquired spectra were phased, baseline-corrected and referenced to lactate signal at δ (1.33 ppm). Spectra were processed with an adapted version of Dolphin (21) for automatic targeted metabolite profiling and quantification. Several database engines (BBioref AMIX database (Bruker), Chenomx and HMDB (22) were used for 1D-resonances assignment and metabolite identification.

Real-time PCR – Quantitative real-time PCR of parental, CSC and chemoresistant cell lines was used to determine levels of the following stem/EMT related genes: Nanog (Hs04399610_g1), Oct3/4 (Hs04260367_gH), Klf4 (Hs00358836_m1), ABC (Hs01059137_m1), Sox2 (Hs01053049_s1), Snail (Hs00161904_m1), Twist (Hs01675818_s1), ALDH1 (Hs00946916_m1) and housekeeping genes TBP (Hs00427620_m1) and IPO8 (Hs00183533_m1). Assays-on-Demand Taqman Gene Expression Assays (Applied Biosystems, Foster City, CA, USA) was used according to the procedure previously described (23).

Cell metabolic activity assay – Cell metabolic activity was assessed by 3-(4,5-dimethylthiazol-2-yl)-5-(3-carboxymethoxyphenyl)-2-(4-sulfophenyl)-2H-tetrazolium (MTS) assay (Promega, CellTiter 96® MTS Reagent Powder, G111A; Sigma, Phenazine methosulfate, P9625) in 96-well plates by adding MTS reagents to 10.000 cells per well. The absorbance was measured at 490nm and results were normalized by protein content using a bicinchoninic acid assay (BCA, Thermo Fischer Scientific, 23225).

Mitochondrial membrane potential (Δψm) – Measurement of Δψm was performed essentially as described in Kumari *et al* (24). Briefly, 15 000 adherent cells were incubated with 1 mM of the mitochondrial potential sensor 5,5,6,6 - tetrachloro1,1,3,3-tetraethylbenzimidazolylcarbocyanine iodide (JC-1, Sigma, T4069). Red (JC-1 aggregate) and green (JC-1 monomers) fluorescence intensities were measured simultaneously using a Thermo Scientific Appliskan microplate reader (Thermo Scientific, Madrid, Spain) at 495/590-nm and 475/530-nm excitation/emission lengths, respectively, followed by adjustment to the blank controls.

Intracellular and mitochondrial ROS – Measurements of intracellular ROS were based on the ability of cells to oxidize fluorogenic dye 2',7'-dichlorofluorescein (H2DCF-DA) to their corresponding fluorescent analogues, that allowed ROS determination in living cells (24). Mitochondrial ROS was detected by measuring mitochondrial superoxide with MitoSOX red reagent according to the manufacturer's protocol (Invitrogen, Thermo Scientific, M36008).

Measurement of ATP level – ATP level was measured using ATPlite kit as described in the manufacturer's manual (PerkinElmer, 6016943). A solution of 10.000 cells in 100 ul media/well was plated in triplicates in a black 96-well plate with clear bottom. 50ul of reagent was added to each well and the plate was mixed for 5 min on an orbital shaker to induce cell lyses followed by incubation in the dark for 10 min to stabilize luminescence. The ATP content was then measured with Biotek's Synergy Mx luminometer.

OCR measurement with Seahorse XFe-24 analyzer – To measure OCR, the Seahorse apparatus (Agilent Technologies Spain, S.L.) was utilized. In short, 50.000 cells per well were seeded in triplicates or quadruplicates into XFe-24 well

plates and treated with antibiotics. After 72 hours of treatment, cells were washed with PBS 1x and pre-warmed XF assay media (Agilent, 102353-100), supplemented with 5,5 mM glucose, 2 mM pyruvate and 2 mM L-glutamine was added to each well. Cells were then maintained at 37ºC in a non-CO2 incubator for 1 hour. Cell Mito Stress Test kit was utilized to measure mitochondrial parameters by XF24 Analyzer. Measurements were normalized with a posterior BCA assay.

Mitochondrial complex activity measurement – The activity of mitochondrial OXPHOS Complex I (NADH dehydrogenase) and Complex III were measured with kits (ab109721 and ab109905, respectively, both from Abcam, UK) according to the manufacturer's manual. The specific enzymes were immunocaptured within the wells of the 96 well microplate. Complex I activity was determined following the oxidation of NADH to NAD+ and the simultaneous reduction of a dye which leads to increased absorbance at OD=450 nm. The activity of complex III was measured using the following formula provided in the Manufacturer´s manual: CIII activity = Rate sample – Rate background (row A/H). Complex III activity is proportional to the increase in absorbance at OD 550 nm examined in the linear phase of the reaction progress curves.

Plasmid transfection and detection of LC3 foci and mitophagic events – The plasmid pRFP-LC3 (AddGene) was transfected with Lipofectamine 2000 (Thermofisher, 11668027) according to the manufacturer's instructions. After 1d, corresponding cells were plated on slides and treated with selected antibiotics for 72h. Cells were stained with Hoechst dye, fixed and analyzed by confocal microscopy (Nikon 1 AR inverted Microscope, 40 objectives, 561 nm excitation

length). At least 10 cells per slides were analyzed and the average number of RFP-LCR puncta per cell was counted.

Western blotting and sample preparation – Analyses was performed essentially as described in Kumari et al (24). Samples were equilibrated for protein using a BCA assay and lysates were separated on 4-20% acrylamide gels, blotted on nitrocellulose membranes and incubated overnight with the appropriate primary antibodies: NANOG (#560109), SOX2 (#561469), OCT4 (#611202), all from BD, USA; b-actin, p62 (#8025), LC3ab (#3868), m-TOR (#2972), p-mTOR (#5536), Atg5 (#9980), Atg7(#2631), mtMarkers (#8674) (from Cell Signaling), GAPDH (sc-32233), POLG (sc-390634), RPS3 (sc-376098), MRPS6 (sc-390597), MRPS23 (sc-514827), all from SantaCruz Biotechnology, USA, followed by detection with corresponding HRP-conjugated secondary antibodies (Sigma). Samples and data from patients included in this study were provided by the Tumor Bank of Vall d'Hebron University Hospital Biobank (PT13/0010/0021), integrated in the Spanish National Biobanks Network and Xarxa de Bancs de Tumors de Catalunya (XBTC), and they were processed following standard operating procedures with the appropriate approval of the Ethical and Scientific Committees.

Colony formation assays – The assay was performed essentially as described previously (25). Cells were suspended in colourless DMEM media containing 0,2 % agarose in the presence or absence of antibiotics and layered in triplicates over a solid base of 0,6% agarose in 6 well plates. Cells were incubated at 37^0C for 2 weeks and the average number of colonies per well was counted.

Immunohistological (IHC) analyses – The expression of p62 (SAB3500430, Sigma), Ki67 (NCL-L-Ki67-MM1, Leica Biosystems), and LC3 (3868, Cell

Signaling) proteins were studied by IHC in mice xenografted tumour samples. Sections from paraffin-embedded samples were incubated overnight at 4ºC with the indicated antibodies (1:50, 1:200, 1:200 and 1:500 for LC-3, P62, Ki67 and Caspase3, respectively) and the immunostaining was performed using the ChemMate DAKO EnVision Detection Peroxidase/DAB kit (K4065, DAKO Diagnostic). All sections were counterstained with Harris' Haematoxylin and mounted with DPX.

Animals xenograft models – Ethical committee approval has been obtained prior to the experiments (CEEA Vall d'Hebron Institut de Recerca (VHIR)). Young adult (5-9 weeks) female NMRI-nu mice were purchased from Janvier Labs (France) and housed in a pathogen-free environment. Animals were s.c. inoculated in the flank with $1x10^5$ cells mixed with matrigel of either 231-Par, 231-Rcyclo or 231-CSC. Mice were housed in groups of 5 and randomly assigned to treatments. Linezolid was administered at a concentration of 100 mg/kg/day as described in Patel *et al* (26) and HCQ at 50 mg/kg/day (27). Weight and tumour growth (measured with a calliper and using the formula [length (mm) x $width^2$ (mm)]/2) were followed semi-weekly.

Results:

Functional mitochondria are implicated in common metabolic pathways among CSC, chemoresistant and breast cancer cells

In order to understand the differences in the metastatic capacity already described for CSC and chemoresistant cancer cells (5–7) in comparison to the parental cancer cells, we have created several corresponding models based on TNBC cell lines, in particular MDA-MB-231, in their resistance to

cyclophosphamide, cisplatin and doxorubicin. In order to create CSC-like cells, parental cells were resuspended in non-adherent conditions with a stem cell media to form tumourspheres. We recognized, that both CSC and chemoresistant cancer cells displayed increased expression of stem cell markers NANOG, Sox4, KLF4 and Oct4 in comparison with the isogenic parental counterparts, suggesting overlapping regulated pathways (Fig. S1A, B). We also noticed that metastatic capacity of resistant cancer cell lines is much higher than that of parental counterparts as they formed significantly higher number of tumorspheres (Fig. S1C). We then performed quantitative proteomic analyses of these cells and identified significantly overexpressed and underexpressed proteins in chemoresistant cells or CSC as compared to their corresponding parental cancer cells (Fig. 1 and Table S1). The proteomics data were recapitulated for another TNBC cell line, BT549 (not shown). Interestingly, cancer cells resistant to cyclophosphamide (Fig. 1A), cisplatin (Fig. 1B) or doxorubicin (Fig. 1C), shared differentially expressed proteins with CSC (Fig. 1A-C). To determine the characteristics of these differentially expressed proteins, Reactome pathway analyses of up-regulated and down-regulated proteins were performed. Remarkably, among top altered pathways, our results revealed those involved in metabolic reprogramming, TCA cycle or respiratory chains (Fig. 1D). Western blot analyses revealed upregulation of several mitochondrial proteins as well as those involved into TCA cycle (Fig. 1E). Similar upregulation of respiratory complexes I-V were obtained in a panel of triple negative breast tumours, known to be more aggressive and more chemoresistant than the other types of TNBTs (Fig. 1F and Fig. S2). In parallel, we performed NMR-based quantitative metabolomics analyses of these cells and demonstrated significantly increased

levels of metabolites in chemoresistant cells or CSC as compared to their corresponding counterparts (Fig. 1G,H). In summary, our data provide compelling evidence that metabolic activities of CSC and cancer resistant cells are higher than in corresponding parental cells, and are likely due to the increased activities of mitochondria.

MDF-inducing bactericidal antibiotics inhibit the growth of cancer cells and discriminate CSC and resistant cancer cells from parental counterparts

Induction of MDF can in principle, disrupt OXPHOS, following energy depletion of cancer cells and suppression of cancer cell growth. In order to test this hypothesis, we have performed an *in vivo* experiment on mice xeno-injected with MDA-MB-231 Rho^0 and MDA-MB-231 chemoresistant Rho^0 cancer cells, both having MDF. In parallel, a control group of mice was xeno-injected with MDA-MB-231 parental or chemoresistant cancer cells having functional mitochondria. Our results clearly demonstrated that growth of tumours was significantly delayed in mice injected with cancer cells having MDF, as compared to the control group (Fig. 2). This indicates that MDF-inducing agents can be utilized as potential anticancer drugs.

Ours and other recent works revealed that specific antibiotics might cause MDF in eukaryotic cells and decrease cancer cell growth (16, 19). In order to address this question to our model, cancer cells have been screened over a panel of antibiotics to identify those that decrease cell growth (Fig. 3A). Similar results were observed for the pharyngeal carcinoma cell line CCL-138/Detroit-562 (Fig. S3B). We have selected linezolid and hygromycin B, as the drugs decreasing metabolic activities of several types of cancer cells, including TNBC cell lines. In addition, the selected antibiotics were able to suppress cancer cell growth *in vitro*

(Fig. 3A) and increased apoptosis (Fig. 3B). Profiling of major mitochondrial complexes demonstrated significant decrease in expression levels of proteins corresponding to respiratory complexes and suggested that antibiotics predominantly suppress CSC and resistant cells rather than parental counterparts (Fig. 3C). We then tested for the ability of these antibiotics to induce MDF. For that part, we have measured major mitochondrial parameters, including mitochondrial membrane potential (Fig. 3D), activities of mitochondrial complexes (Fig. 3E and 3F), routine oxygen consumption rate (OCR) (Fig. 3G and Fig. S4) and ATP levels (Fig. 3H). These results suggest that specific bactericidal antibiotics inhibiting metabolic activity of cancer cells also reduce cancer cell growth, possibly by inducing MDF.

MDF-inducing bactericidal antibiotics reduce tumour growth

In order to study the role of MDF-inducing antibiotics on tumorigenic properties of cancer cells in details, we have performed colony-formation assays and demonstrated that both antibiotics reduced the tumorigenic capacities of CSC, parental, and to a less extent chemoresistant MDA-MB-231 cells (Fig. 4A). Next, we demonstrated that treatment with either of selected antibiotics decreased formation of tumourspheres (Fig. 4B). These and *in vitro* findings on growth inhibition of cancer cells, prompted us to provide animal studies. First, we performed a pilot experiment to determine physiologically appropriate concentrations of one of the drugs, linezolid, which previously demonstrated a suppressive role in mitochondrial functions (19). Then, we performed xeno-injection of immunocompromised mice with either CSC, chemoresistant or parental cancer cells and allowed tumours to grow for 3 weeks, as described in the flowchart (Fig. 4C). Linezolid or placebo were orally administrated to the mice

for 3 weeks and the tumour rates were monitored twice a week. Our results provided compelling evidences that linezolid significantly reduced tumour growth rate (Fig. 4D-F and Fig. S5). Notably, this antibiotic revealed higher antitumour activity both for chemoresistant and CSC, in comparison with parental cancer cells as revealed by comparing average velocities of tumour growth. Immunohistochemical staining with the proliferative marker Ki-67 from corresponding tumour sections demonstrated an antibiotic-dependent decrease in proliferation rate (Fig. 4G and Fig. S6). This corroborates well with our previous observations on alterations of metabolic pathways among these types of cells (Fig. 1). With the idea of observing if the decrease in the proliferation rate correlated with defective mitochondrial respiration, we have performed SeaHorse experiments in the cells from extracted tumours grown in antibiotic-free media for more than 10 days. Surprisingly, we found that cells obtained from linezolid-administered mice demonstrated a decrease in OCR (Fig. S7). In totality, these data suggest that linezolid may reduce tumour growth rate and discriminate resistant and CSC from the parental counterparts.

MDF-inducing antibiotics decrease mitoribosomal translation, inhibit syntheses of metabolites, increase intracellular ROS and enhance autophagy

Recently, the anticancer activity of bactericidal antibiotics in cell cultures and in animal models were associated with increased ROS levels (16). First, we tested the possibility that selected antibiotics affect translation of mitoribosomes. Indeed, a decrease in signals from mito- but not cyto-ribosomal proteins confirmed this assumption (Fig. 5A). In addition, we have performed NMR-metabolomic profiling and demonstrated that antibiotics substantially inhibited

production of intracellular metabolites, especially in CSC and in chemoresistant cells (Fig. S8). MDF often leads to overproduction of ROS. In order to understand whether selected antibiotics elevate ROS levels in our cell models and whether this may affect cancer cell survivability, we have measured ROS in CSC, resistant and parental cancer cells. Exposure of all three cell types to either linezolid or hygromycin B significantly increased intracellular (Fig. 5B) and mitochondrial ROS levels (Fig. 5C).

It has been described that oxidative stress accompanied by the non-specific post-translational modifications of proteins, protein aggregation and MDF may contribute to autophagy (19). For that reason, we have tested in our cell models whether antibiotics increasing ROS would induce autophagy. Our data demonstrated that both antibiotics increase autophagic events, presumably in CSC and resistant cancer cells, as revealed by accumulation of modified LC3 protein, decreased activity of mTOR (Fig. 5D), increased p62, Atg5, Atg7 levels (Fig. S9 and Table S1), as well as by the increase of the LC3 autophagic foci formation (Fig. 5E). Moreover, immunohistochemical data from the tumours extracted from mice treated with linezolid revealed an increase in p62 and LC3 staining as compared to the placebo (control) treated mice tumours, validating autophagy increase *in vivo*, upon treatment with antibiotics (Fig. 5F and Fig. S10). Although both linezolid (Fig. 5G) and hygromycin (not shown) had a very little effect on ROS in corresponding Rho^0 cells, exposure of cells with a combination of ROS scavengers followed by antibiotic treatment was able to reverse the autophagy induction provoked by antibiotics suggesting that autophagy is partially caused by the antibiotic-mediated ROS increase (Fig. 5H). Thus far, our

studies suggest that antibiotics interfering with mitochondrial function increase intracellular and mitochondrial ROS and induce autophagy in cancer cells.

Simultaneous treatment with MDF-inducing antibiotics and autophagy blocker reduce the metastatic capacity of CSC and resistant cancer cells

Provided that treatment with MDF-inducing antibiotics increased overall autophagy levels, presumably in CSC and chemoresistant cells (Fig. 5 and Fig. S9), we hypothesized that dysfunctional mitochondria can be eliminated by autophagy in a long term and autophagy itself could promote cancer cell proliferation and tumour outgrowth. If so, treatment with autophagy inhibitors may amplify the effects of antibiotics by increasing MDF. For testing such assumption, we have identified areas of synergy in MDA-MB-231 cell line across a wide range of concentrations of linezolid and autophagy blocker, hydroxychloroquine (HCQ). We used BCA assay and calculated Loewe and Bliss drug synergy scores using Combenefit software (28). We identified areas of synergy in MDA-MB-231 cell line (Fig. S11). In order to confirm the synergy between linezolid and HCQ in a different assay system, we used a soft-agar colony formation assay for the cells treated with antibiotics or in combination with autophagy blocker, hydroxychloroquine (HCQ). Notably, adding HCQ sensitized all three cultures to linezolid with additive effects of HCQ to linezolid as 34%, 51% and 26% for 231-Par, 231-Rcyclo and 231-CSC, respectively (Figure 6A-C). In addition, antibiotics and HCQ synergistically inhibited tumoursphere formation (Fig. 6D). Finally, xenotransplantation studies revealed that combinatorial treatment of linezolid with HCQ decreased tumour growth rates (Fig. 6E-G).

Overall, our results provided a framework for multitarget therapy, including the antibiotic treatment in combination with autophagy blockers with a complete understanding of the relevant molecular pathophysiology.

Discussion:

How to cope with the acquisition of resistance is a major challenge in oncology since, in general terms, cancer is 80% curable when it is a primary tumour. The problem arises when a tumour cell learns to be insensitive to the chemotherapeutic agent by developing mechanisms of resistance. Both, resistant variant and CSC, have a higher metastatic ability in the organism (5–7). This fact adversely affects the guarantee of a cure for cancer patients. With the idea of discovering proteins involved in the acquisition of resistance, we carried out a proteomic analysis of resistant cells generated at our laboratory (MDA-MB-231 resistant to cyclophosphamide, cisplatin and doxorubicin). We chose a cellular model of particularly aggressive breast cancer designated as TNBC as in contrast to other molecular variants (Luminal A/B or HER2+), TNBC is often detected at an advanced stage and 50% of patients do not respond to conventional treatment evolving fatally. Interestingly, proteomic and metabolomics studies revealed different pathways that cross-talk with mitochondria. The involvement of the metabolites shown at Fig. 1G improving mitochondrial quality and increasing or maintaining mitochondrial activity has been described in different models (29). Importantly, the known Warburg effect in cancer –measured by high glucose consumption and lactate release- provoked by glycolytic stromal fibroblasts, increased mitochondrial activity in adjacent breast cancer cells *in vivo* (30). Recent findings implies that the disruption of mitochondrial energy metabolism tightly coupled with organelle function should lead to a decrease in overall

metabolic activity (31) and even discriminate resistant cancer cells (32). In fact, we demonstrated that mitochondria defective Rho^0 cells significantly delayed cancer onset. One of the approaches to induce MDF and deplete energy supply for cancer cells is to target mitochondria using antibiotics (18, 19). Indeed, mitochondria that originally evolved from bacterial cells should be sensitive to some antibiotic (18). First, we have screened a panel of antibiotics and identified those that decreased proliferation of MDA-MB-231 cells. For our further experiments we chose linezolid and hygromycin B, both drugs are known to interfere with ribosomal translation by competing for the peptidyl transferase or tRNA-ribosomal acceptor sites of bacterial ribosomes (24–27). Unlike tetracyclin, these drugs display better pharmacokinetics and reveal fewer side-effects. We found that higher sensitivity of CSC and chemoresistant cancer cells to selected antibiotics in comparison to parental cells was accompanied by inhibiting translation of mitoribosomes, suppression of metabolic activity and significant MDF, including a decrease in mitochondrial membrane potential, activities of respiration complexes I and III, ATP level and OCR. Importantly, we recapitulated our *in vitro* data in mice models representing the cellular and molecular changes associated with the initiation and progression of human cancer. This revealed that treatment with linezolid significantly decreased tumour growth. On the other hand, MDF and damaged mitochondria are the main contributors of ROS production (33). In addition, overproduction of ROS may disrupt organelles ability to control redox balance thus increasing the amount of intracellular ROS (34). Previous results performed from our laboratory on CAL51 breast cancer cells treated with antibiotics of different classes also supported these findings (19). In order to explore the effect of antibiotics on ROS production, we studied total and

mitochondrial ROS in the three cell types: parental, resistant and CSC. From such experiments we observed that: i) basal ROS levels are higher in resistant cells (to cyclophosphamide and cisplatin) -but not in CSC- in relation to parental cells and ii) cellular and mitochondrial ROS levels are increased in resistant cells treated with antibiotics versus untreated controls. Specifically, CSC only increase ROS under the action of linezolid but not hygromycin B. The fact that Rho^0 cells do not show ROS increase after antibiotics treatment (Fig. 5E) confirms that production of ROS is mediated by mitochondria. Moreover, we found that the increase in ROS levels induced autophagy in resistant cells, and to a lesser extent in CSC treated with antibiotics, an effect that is reversed by the treatment with the ROS scavenger mix. Although in some circumstances, autophagy suppresses tumorigenesis; in other contexts, autophagy promotes tumour growth (28, 35). Cancers can up-regulate autophagy to survive microenvironmental stress and to increase growth and aggressiveness (36). Therefore we hypothesize that autophagy induction in our model could facilitate tumorigenesis. To avoid this, concomitant treatment of an autophagy blocker (i.e., HCQ) with antibiotics, should prevent autophagy from acting as a tumour survival factor, specifically for those tumours which rely on resistant cancer cells or CSC for progression and recurrence. In our experimental settings, concomitant treatment using linezolid with HCQ was able to decrease tumour size in mice and colony formation in parental, resistant and CSC in comparison with linezolid treatment alone. Intriguingly, HCQ did not show any effect by itself in reducing either the number of colonies or tumour size in mice. Recently, HCQ has been shown to regulate histone acetylation events in breast cancer cells serving as a mediator of epigenetic events (37). It is well possible that at a low

concentration, HCQ is ineffective alone but may work synergistically when applied with antibiotics.

Of relevance, certain chemotherapeutic agents such as cisplatin, have been reported to induce a mitochondrial-dependent ROS response that significantly enhances its action of nuclear damage (38). This suggests that a combination of antibiotics with commonly used anticancer agents (different from autophagy blockers) might also increase their cytotoxic effects.

Overall, our results suggest that combined treatment of cancers, using antibiotics along-side chemotherapy can effectively increase the therapeutic effects against cancer. Importantly, such benefit promise to have a most pronounced effect on particularly aggressive cancer cell variants such as resistant cancer cells or CSC in TNBC. The fact that other cancer cell types, particularly aggressive cancer cell variants, such as CCL-138 and BT549 cell line, are also sensitive to the action of antibiotics, suggests that our results can be applied to different cancer types. Moreover, antibiotics seem to be part of novel generation drugs to include in adjuvant/concomitantly to chemotherapeutical treatments against cancer, to eliminate the possibility that aggressive cellular variants may remain in some way dormant in the organism to develop and evolve in the future.

We believe that our findings provide rationale for conducting new, randomized controlled trials specifically designed to address the issue of potential effectiveness of the use of bactericidal antibiotics in cancer therapy. Given the fact that most of the antibiotics currently used in clinical practice have been previously approved by the U.S. Food and Drug Administration and/or EU Commission and generally have well-known pharmacokinetics and low toxicity, the requirements needed to repurpose such antibiotics for anticancer therapy are

unlikely to be very strict. With this research, we hope that the implications in the clinics are promising and feasible in the medium-short term.

Acknowledgements

We are very grateful to Josep Castellvi for his help with IHC, Laia S Civit for the technical help with Western blotting. This work was supported by grants from the Instituto de Salud Carlos III: PI17/02087 (AL), PI15/01262 (MLL) and CP03/00101 (MLL) co-financed by the European Regional Development Fund (ERDF) and AECC Founding Ref. GC16173720CARR (MLL); Lyakhovich A is granted by Marie-Curie INCOMED fellowship (GA267128) and Y Garcia-Mayea is granted by the VHIR fellowship. The proteomic part of the work was supported by the project CEITEC 2020 (LQ1601) from MEYS CR. DP and ZZ thank for support of Czech Science Foundation project (no. P206/12/G151). CIISB research infrastructure project LM2015043 funded by MEYS CR is gratefully acknowledged for the financial support of the LC-MS/MS measurements at the Proteomic Core Facility.

Author´s contributions

E.A., A.L., Y.G-M., D.S., D.P. performed the experiments; A.L. designed experiments; E.A., A.L., C.M. directed animal study A.L., E.A., M.E.L drafted the manuscript; A.L., E.A., A.Z., D.P., Z.Z., M.E.L. analyzed the data, A.L., M.E.L. obtained funding. All authors revised and approved the final version of the manuscript.

Data availability

All data are available from the authors upon reasonable request. Proteomics data are available via ProteomeXchange with identifier PXD009442.

Conflict of interest

The authors declare that they have no conflict of interest.

References

1. Wallace, D. C. (2012) Mitochondria and cancer. *Nat. Rev. Cancer* 12, 685–698

2. Warburg, O., and S. M. (1923) Tests on surviving carcinoma cultures. *Biochem Z* 142, 317–33.

3. Warburg, O. (1925) On the formation of lactic acid with growth. *Biochem Z* 160, 307–311

4. Kondoh, H., Lleonart, M. E., Nakashima, Y., Yokode, M., Tanaka, M., Bernard, D., Gil, J., and Beach, D. (2007) A High Glycolytic Flux Supports the Proliferative Potential of Murine Embryonic Stem Cells. *Antioxid. Redox Signal.* 9, 293–299

5. Shiozawa, Y., Nie, B., Pienta, K. J., Morgan, T. M., and Taichman, R. S. (2013) Cancer stem cells and their role in metastasis. *Pharmacol. Ther.* 138, 285–93

6. Morata-Tarifa, C., Jiménez, G., García, M. A., Entrena, J. M., Griñán-Lisón, C., Aguilera, M., Picon-Ruiz, M., and Marchal, J. A. (2016) Low adherent cancer cell subpopulations are enriched in tumorigenic and metastatic epithelial-to-mesenchymal transition-induced cancer stem-like cells. *Sci. Rep.* 6, 18772

7. Croker, A. K., Goodale, D., Chu, J., Postenka, C., Hedley, B. D., Hess, D. A., and Allan, A. L. (2009) High aldehyde dehydrogenase and expression of cancer stem cell markers selects for breast cancer cells with enhanced malignant and metastatic ability. *J. Cell. Mol. Med.* 13, 2236–2252

8. Lleonart, M. E., Abad, E., Graifer, D., and Lyakhovich, A. (2017) Reactive Oxygen Species-Mediated Autophagy Defines the Fate of Cancer Stem Cells. *Antioxid. Redox Signal.*, ars.2017.7223

9. Carnero, A., Garcia-Mayea, Y., Mir, C., Lorente, J., Rubio, I. T., and LLeonart, M. E. (2016) The cancer stem-cell signaling network and resistance to therapy. *Cancer Treat. Rev.* 49, 25–36

10. Bhola, N. E., Balko, J. M., Dugger, T. C., Kuba, M. G., Sánchez, V., Sanders, M., Stanford, J., Cook, R. S., and Arteaga, C. L. (2013) TGF-β inhibition enhances chemotherapy action against triple-negative breast cancer. *J. Clin. Invest.* 123, 1348–1358

11. Lyakhovich, A., and Lleonart, M. E. (2016) Bypassing Mechanisms of Mitochondria-Mediated Cancer Stem Cells Resistance to Chemo- and Radiotherapy. *Oxid. Med. Cell. Longev.* 2016, 1716341

12. Dar, S., Chhina, J., Mert, I., Chitale, D., Buekers, T., Kaur, H., Giri, S., Munkarah, A., and Rattan, R. (2017) Bioenergetic Adaptations in Chemoresistant Ovarian Cancer Cells. *Sci. Rep.* 7, 8760

13. Guerra, F., Arbini, A. A., and Moro, L. (2017) Mitochondria and cancer chemoresistance. *Biochim. Biophys. Acta - Bioenerg.* 1858, 686–699

14. Chen, H., and Chan, D. C. (2017) Mitochondrial Dynamics in Regulating the Unique Phenotypes of Cancer and Stem Cells. *Cell Metab.* 26, 39–48

15. Loureiro, R., Mesquita, K. a, Oliveira, P. J., and Vega-Naredo, I. (2013) Mitochondria in cancer stem cells: a target for therapy. *Recent Pat. Endocr. Metab. Immune Drug Discov.* 7, 102–14

16. Kalghatgi, S., Spina, C. S., Costello, J. C., Liesa, M., Morones-Ramirez, J. R., Slomovic, S., Molina, A., Shirihai, O. S., and Collins, J. J. (2013) Bactericidal antibiotics induce mitochondrial dysfunction and oxidative damage in Mammalian cells. *Sci. Transl. Med.* 5, 192ra85

17. Moullan, N., Mouchiroud, L., Wang, X., Ryu, D., Williams, E. G., Mottis, A., Jovaisaite, V., Frochaux, M. V., Quiros, P. M., Deplancke, B., Houtkooper, R. H., and Auwerx, J. (2015) Tetracyclines Disturb Mitochondrial Function across Eukaryotic Models: A Call for Caution in Biomedical Research. *Cell Rep.* 10, 1681–1691

18. Lleonart, M. E., Grodzicki, R., Graifer, D. M., and Lyakhovich, A. (2017) Mitochondrial dysfunction and potential anticancer therapy. *Med. Res. Rev.* 37, 1275–1298

19. Esner, M., Graifer, D., Lleonart, M. E., and Lyakhovich, A. (2017) Targeting cancer cells through antibiotics-induced mitochondrial dysfunction requires autophagy inhibition. *Cancer Lett.* 384, 60–69

20. Feliciano, A., Garcia-Mayea, Y., Jubierre, L., Mir, C., Hummel, M., Castellvi, J., Hernández-Losa, J., Paciucci, R., Sansano, I., Sun, Y., Cajal, S. R. y, Kondon, H., Soriano, A., Segura, M., Lyakhovich, A., and LLeonart, M. E. (2017) miR-99a reveals two novel oncogenic proteins E2F2 and EMR2 and represses stemness in lung cancer. *Cell Death Dis.* 8, e3141

21. Gómez, J., Brezmes, J., Mallol, R., Rodríguez, M. A., Vinaixa, M., Salek, R. M., Correig, X., and Cañellas, N. (2014) Dolphin: a tool for automatic targeted metabolite profiling using 1D and 2D 1H-NMR data. *Anal.*

Bioanal. Chem. 406, 7967–7976

22. Haug, K., Salek, R. M., Conesa, P., Hastings, J., de Matos, P., Rijnbeek, M., Mahendraker, T., Williams, M., Neumann, S., Rocca-Serra, P., Maguire, E., González-Beltrán, A., Sansone, S.-A., Griffin, J. L., and Steinbeck, C. (2013) MetaboLights—an open-access general-purpose repository for metabolomics studies and associated meta-data. *Nucleic Acids Res.* 41, D781–D786

23. Artero-Castro, A., Callejas, F. B., Castellvi, J., Kondoh, H., Carnero, A., Fernández-Marcos, P. J., Serrano, M., Ramón y Cajal, S., and Lleonart, M. E. (2009) Cold-inducible RNA-binding protein bypasses replicative senescence in primary cells through extracellular signal-regulated kinase 1 and 2 activation. *Mol. Cell. Biol.* 29, 1855–68

24. Kumari, U., Ya Jun, W., Huat Bay, B., and Lyakhovich, A. (2014) Evidence of mitochondrial dysfunction and impaired ROS detoxifying machinery in Fanconi Anemia cells. *Oncogene* 33, 165–172

25. Lyakhovich, A., and Surralles, J. (2006) Disruption of the Fanconi anemia/BRCA pathway in sporadic cancer. *Cancer Lett.* 232, 99–106

26. Patel, M. I., and Makhija, S. J. (2012) Toxicity assessment of Linezolid and the beneficial effects of human erythropoietin in mice. *Eur. J. Exp. Biol.* 2, 2172–2181

27. McChesney, E. W. (1983) Animal toxicity and pharmacokinetics of hydroxychloroquine sulfate. *Am. J. Med.* 75, 11–18

28. Di Veroli, G. Y., Fornari, C., Wang, D., Mollard, S., Bramhall, J. L.,

Richards, F. M., and Jodrell, D. I. (2016) Combenefit: an interactive platform for the analysis and visualization of drug combinations. *Bioinformatics* 32, 2866–2868

29. Zhang, Y., Su, W., Zhang, Q., Xu, J., Liu, H., Luo, J., Zhan, L., Xia, Z., and Lei, S. (2018) Glycine Protects H9C2 Cardiomyocytes from High Glucose- and Hypoxia/Reoxygenation-Induced Injury via Inhibiting PKC *β* 2 Activation and Improving Mitochondrial Quality. *J. Diabetes Res.* 2018, 1–8

30. Migneco, G., Whitaker-Menezes, D., Chiavarina, B., Castello-Cros, R., Pavlides, S., Pestell, R. G., Fatatis, A., Flomenberg, N., Tsirigos, A., Howell, A., Martinez-Outschoorn, U. E., Sotgia, F., and Lisanti, M. P. (2010) Glycolytic cancer associated fibroblasts promote breast cancer tumor growth, without a measurable increase in angiogenesis: Evidence for stromal-epithelial metabolic coupling. *Cell Cycle* 9, 2412–2422

31. Yu, M., Shi, Y., Wei, X., Yang, Y., Zhou, Y., Hao, X., Zhang, N., and Niu, R. (2007) Depletion of mitochondrial DNA by ethidium bromide treatment inhibits the proliferation and tumorigenesis of T47D human breast cancer cells. *Toxicol. Lett.* 170, 83–93

32. Kuntz, E. M., Baquero, P., Michie, A. M., Dunn, K., Tardito, S., Holyoake, T. L., Helgason, G. V., and Gottlieb, E. (2017) Targeting mitochondrial oxidative phosphorylation eradicates therapy-resistant chronic myeloid leukemia stem cells. *Nat. Med.* 23, 1234–1240

33. Murphy, M. P. (2009) How mitochondria produce reactive oxygen species. *Biochem. J.* 417, 1–13

34. Lyakhovich, A., and Graifer, D. (2015) Mitochondria-Mediated Oxidative Stress: Old Target for New Drugs. *Curr. Med. Chem.* 22, 3040–53

35. Lee, J., Giordano, S., and Zhang, J. (2012) Autophagy, mitochondria and oxidative stress: cross-talk and redox signalling. *Biochem. J.* 441, 523–40

36. White, E. (2015) The role for autophagy in cancer. *J. Clin. Invest.* 125, 42–46

37. Rahim, R., and Strobl, J. S. (2009) Hydroxychloroquine, chloroquine, and all-trans retinoic acid regulate growth, survival, and histone acetylation in breast cancer cells. *Anticancer. Drugs* 20, 736–745

38. Marullo, R., Werner, E., Degtyareva, N., Moore, B., Altavilla, G., Ramalingam, S. S., and Doetsch, P. W. (2013) Cisplatin induces a mitochondrial-ROS response that contributes to cytotoxicity depending on mitochondrial redox status and bioenergetic functions. *PLoS One* 8, e81162

Figure Legends

Fig. 1. Quantitative omics analyses revealed overlapping regulated metabolic pathways among resistant, CSC and parental triple-negative breast cancer cells. Differentially expressed up- and down-regulated proteins between MDA-MB-231 parental (231-Par) and corresponding CSC (231-CSC) or chemoresistant cells (231-R) were identified by quantitative proteomics. Overlapping differentially expressed proteins between CSC and cancer cells chemoresistant to (A) cyclophosphamide, (B) cisplatin and (C) doxycycline, are shown on Venn diagram. (D) The top 10 significantly enriched up- and down-regulated biological processes, as analyzed by Reactome program, are shown on the middle panel. Asterisk signifies processes related to mitochondrial biology. (E) Western blot analyses of proteins from major mitochondrial complexes and metabolic pathways. (F) Expression of proteins from major mitochondrial complexes in the samples of TNBT (n=11) versus paired non-tumoural adjacent tissues (n=11). Statistical analyses was done with Mann-Whitney test. (G) NMR-based quantitative metabolomic analyses shows elevated levels of metabolites in 231-CSC, 231-R and 231-Par cells. The value of each bar represents pic square of corresponding metabolites normalized to the total number of cells in the sample. (H) NMR spectra of individual metabolites obtained for the samples of 231-CSC, 231-R and 231-Par cells.

Fig. 2. Delayed tumour growth correlates with MDF. (A) Rho^0 cells were created by poisoning corresponding cells with ethidium bromide causing mtDNA depletion, as revealed by semi-quantitative PCR and Western blotting, showing absence of *PolG* and decreased POLG, respectively. (B) Flowchart describing the scheme of animal experiments. (C) Mice (n=5) were xeno-injected with $1x10^6$

parental and parental Rho^0 cells or (D) cyclophosphamide chemochemoresistant and chemoresistant Rho^0 cells and tumour volumes have been measured 4 weeks after injection. Data represent the mean ± SD. (E) Representative pictures of mice demonstrate differences in tumour growth after 3 weeks upon xeno-injection.

Fig. 3. The effects of bactericidal antibiotics on the cell survivability and on the mitochondrial functions. (A) MDA-MB-231 cells and corresponding CSC and chemoresistant cells have been treated with linezolid or hygromycin B, and cell survivability was measured following indicated time intervals. Results represent the mean +/- SD. (B) Apoptosis was measured by Annexin V-PE using FACS in of DMSO control or the predetermined IC25 values of Linezolid and Hygromycin B induced for 72 hours. (C) Expression levels of mitochondrial proteins revealed by Western blot analyses of corresponding cell fractions treated or untreated with antibiotics for 72 hours. Below are signals normalized to b-actin. (D) Mitochondrial membrane potential was measured using JC1 dye. (E) Function of ETC protein complexes I and (F) III were measured spectrofluorimetrically using with kits ab109721 and ab109905, respectively (both from Abcam). Bars represent the change in activity of individual antibiotic-treated complexes compared to untreated complexes. (G) OCR rates have been measured based on SeaHorsex24 experiments (Supplementary Figure 3a). (H) ATP levels (Complex V) were measured using a luciferin/luciferase assay. Comparisons between treatments and untreated controls were made using a Student's t test (*P < 0.05, **P < 0.01, ***P < 0.001).

Fig. 4. MDF-inducing antibiotics reduce tumorigenic properties of cancer cells and tumour growth rate. (A) Quantifications of soft-agar colony-formation

assays of MDA-MB-231 parental, chemoresistant to cyclophosphomide cancer cells and CSC, following treatment with linezolid for 72 hours. Data represent the mean ± SD. Representative images of colonies are shown above. (B) Quantifications of tumoursphere-formation assays of MDA-MB-231 CSC, following treatment with linezolid or hygromycin B for 9 days. Data represent the mean ± SD. (C) Flowchart describing the scheme of animal experiments. Mice (n=5) were xeno-injected with $1x10^6$ (D) parental, (E) chemochemoresistant or (F) CSC MDA-MB-231 cells followed by oral administration with placebo (black line) or with linezolid (red line). (*P < 0.05, **P < 0.01). Tumour size was monitored semiweekly and corresponding rates were plotted onto the diagram. Average velocities (AV) of tumour growth are shown for each groups of mice. Data represent the mean ± SD. (G) Immunohistochemical analysis of Ki-67 proliferation marker with the percentage of Ki-67 positive nucleus is depicted on each slide. Positive and negative controls are shown on the right side.

Fig. 5. Antibiotics induce inhibition of mitoribosomal translation followed by decrease metabolic activity and mitochondria-mediated ROS increase in cancer cells. (A) Antibiotic-induced inhibition of mitoribosomal but not cytoribosomal translation was evaluated by Western blot analysis as revealed by decreased expression of mitoribosomal proteins MRPS23 and MRPL6 (% of signal intensities are shown below each blot). (B) Total ROS were measured in corresponding MDA-MB-231 cells after 3 days of exposure to linezolid (100 µg/ml) and hygromycin B (150 µg/ml)] compared to untreated cells. ROS was quantified using CM-H2DCFDA by fluorescent microplate spectrophotometer. (C) Mitochondrial superoxide was measured using MitoSox Red. (D) Antibiotic-induced autophagy markers were evaluated by Western blot analysis. (E) Cells

have been transformed with LC3-RFP pDNA, followed by treatment with corresponding antibiotics. Representative immunofluorescent pictures demonstrate accumulation of LC3 puncture staining. Corresponding bar diagram displays average number of LC3 puncture per cell, as revealed by immunofluorescence analyses. All bar graphs indicate means ± SEM (n ≥ 10). Comparisons between treatments and untreated controls were made using a Student's t test ($P < 0.05$). (F) LC3 and p62 staining of tumour biopsies extracted from mice orally administrated with placebo or linezolid revealed increased autophagy. (G) ROS were also measured in mtDNA depleted Rho^0 cells treated or untreated with antibiotics. Hydrogen peroxide treated cells were used as positive controls. Data represent the mean ± SD. (H) Exposure of antibiotic-treated MDA-MB-231 cells to the ROS scavengers reduced autophagy, as revealed by decreased ratio of modified LC3II vs LC3I signals. Comparisons between treatments and untreated controls in panels B,C,E,G were made using a Student's t test (*$P < 0.05$, **$P < 0.01$, ***$P < 0.001$).

Fig. 6. Simultaneous treatment with MDF-induced antibiotic and autophagy blocker reduced metastatic capacity of cancer cells and tumour growth rate. Quantifications of soft-agar colony-formation assays of MDA-MB-231 parental (A), resistant (B) and CSC (C) following 72 hours treatment with linezolid (Lin) or hygromycin B (Hygro), in the presence or absence of HCQ. (D) Quantifications of tumoursphere-formation assays of MDA-MB-231 CSC, following treatment with linezolid or hygromycin B for 9 days. Data represent the mean ± SD. Mice (n=5) were xeno-injected with $1x10^6$ parental (E), chemoresistant (F) or CSC MDA-MB-231 cells (G) and allowed tumours to form for 3 weeks. Mice were orally administrated with placebo (Cont), linezolid (Lin),

HCQ, or combination of both (Combo) and tumour rates were calculated as shown on the diagram. Data represent the mean ± SD. Comparisons between treatments and untreated controls were made using a Student's t test (*P < 0.05, **P < 0.03, ns - nonsignificant).

Figures

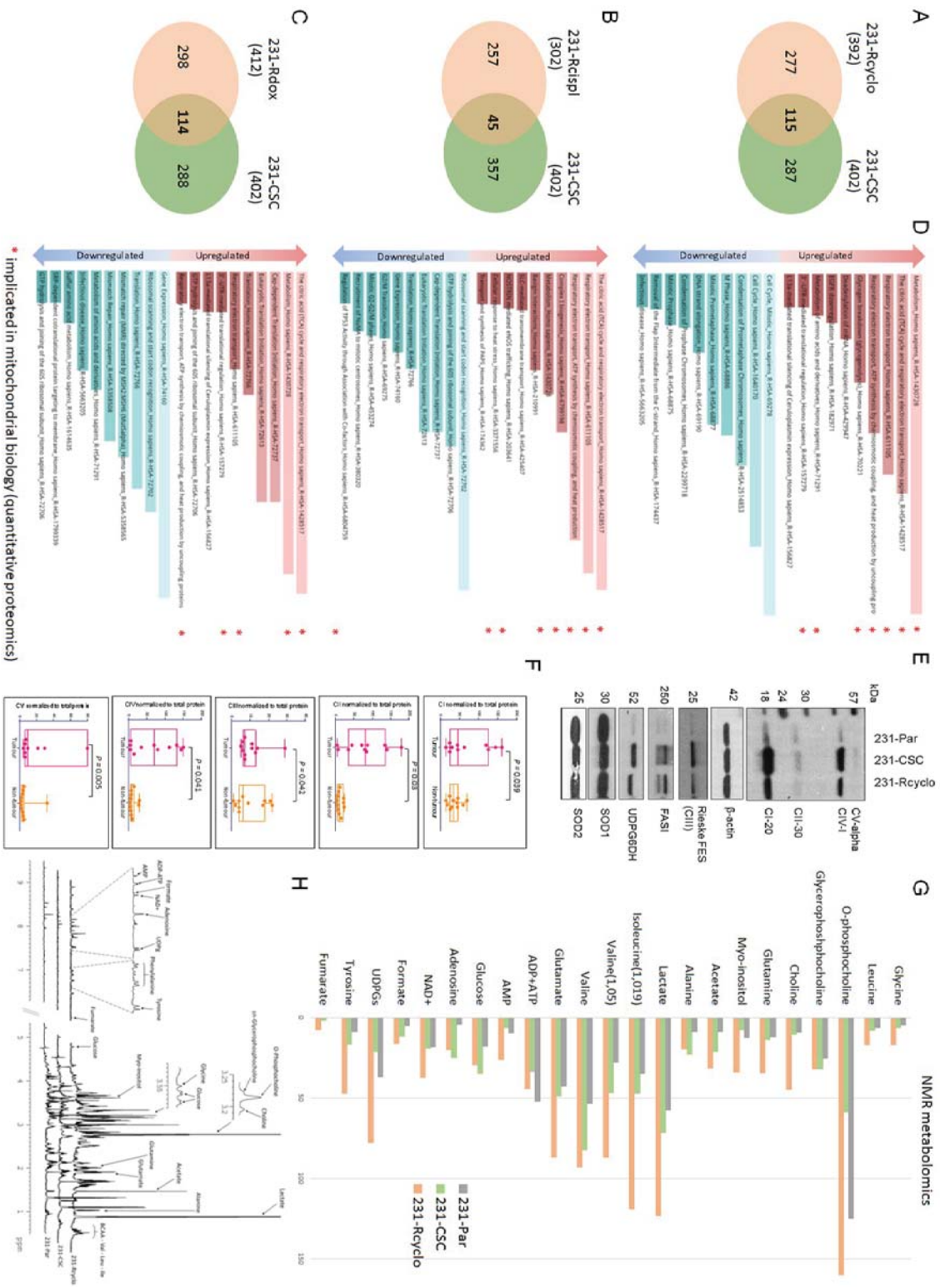

Fig. 1 (page 16)

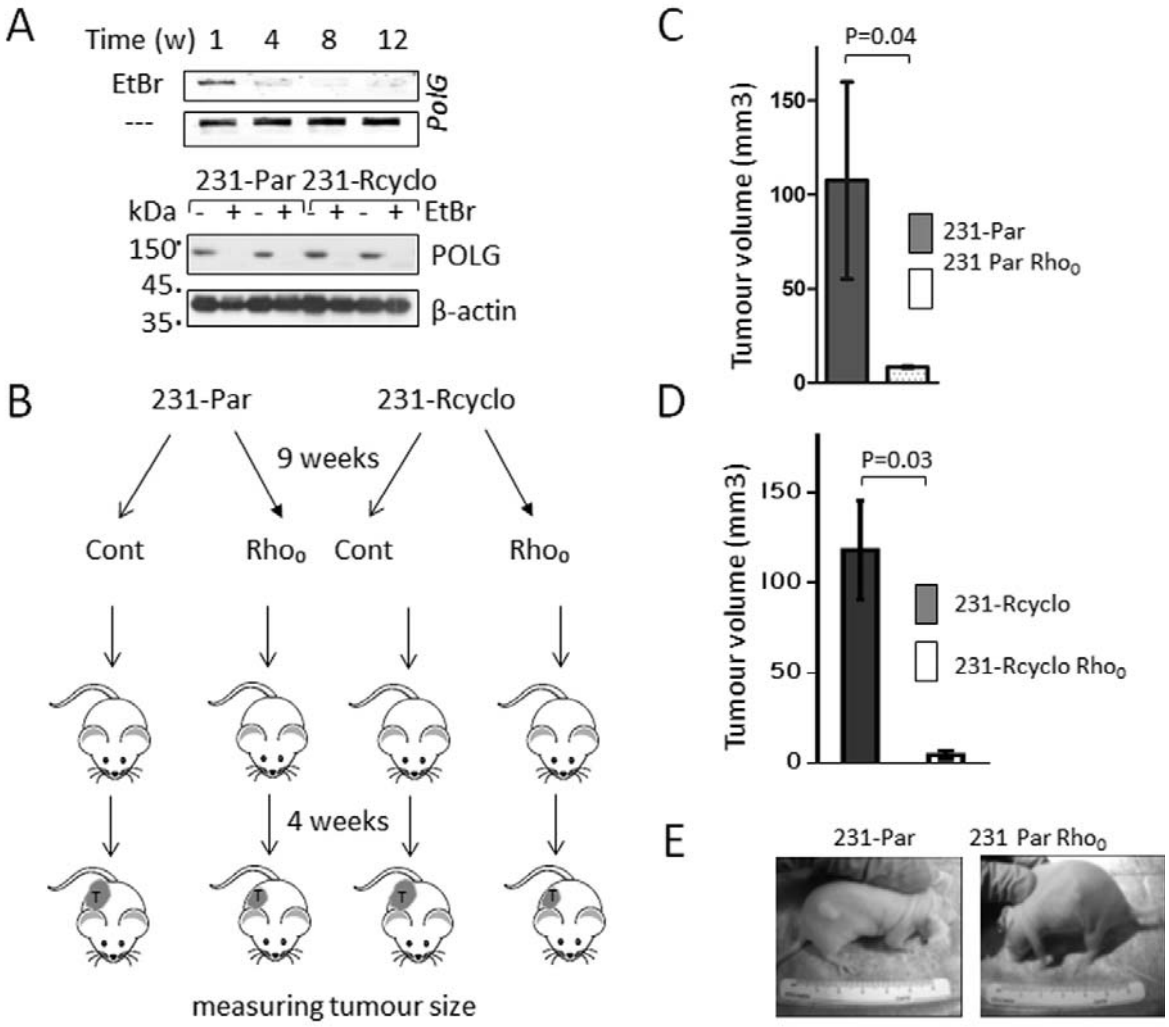

Fig. 2 (page 17)

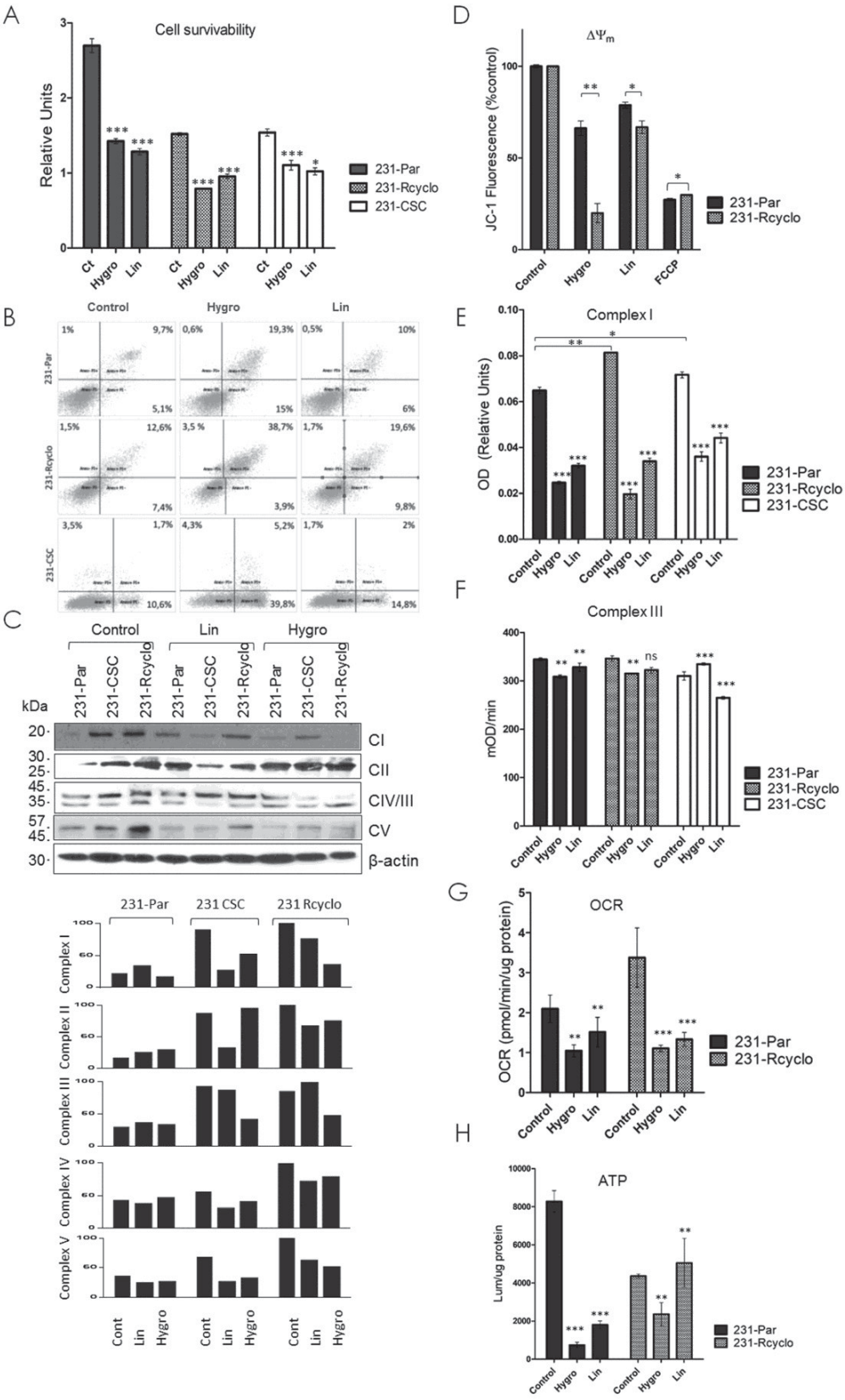

Fig. 3 (page 18)

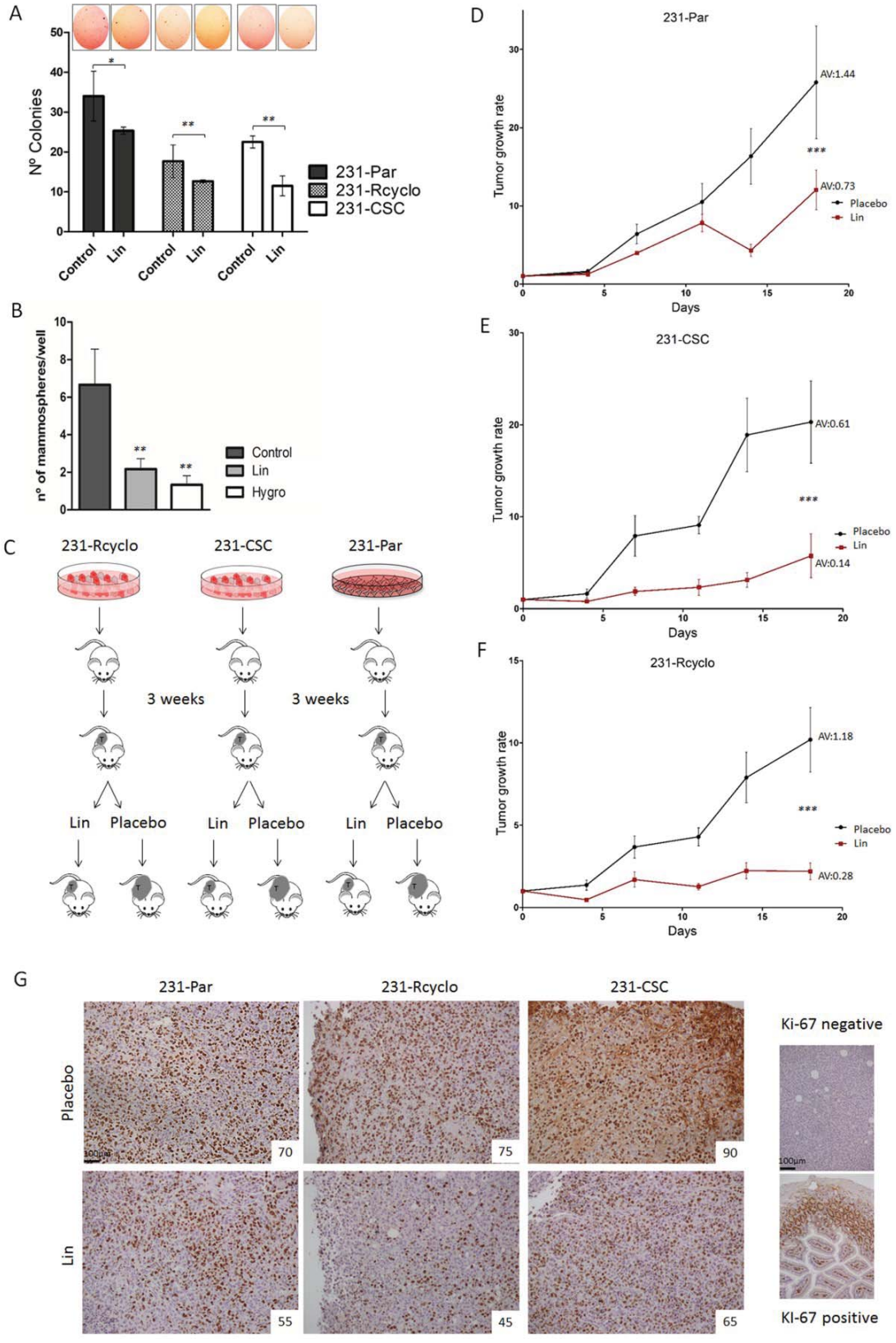

Fig. 4 (page 19)

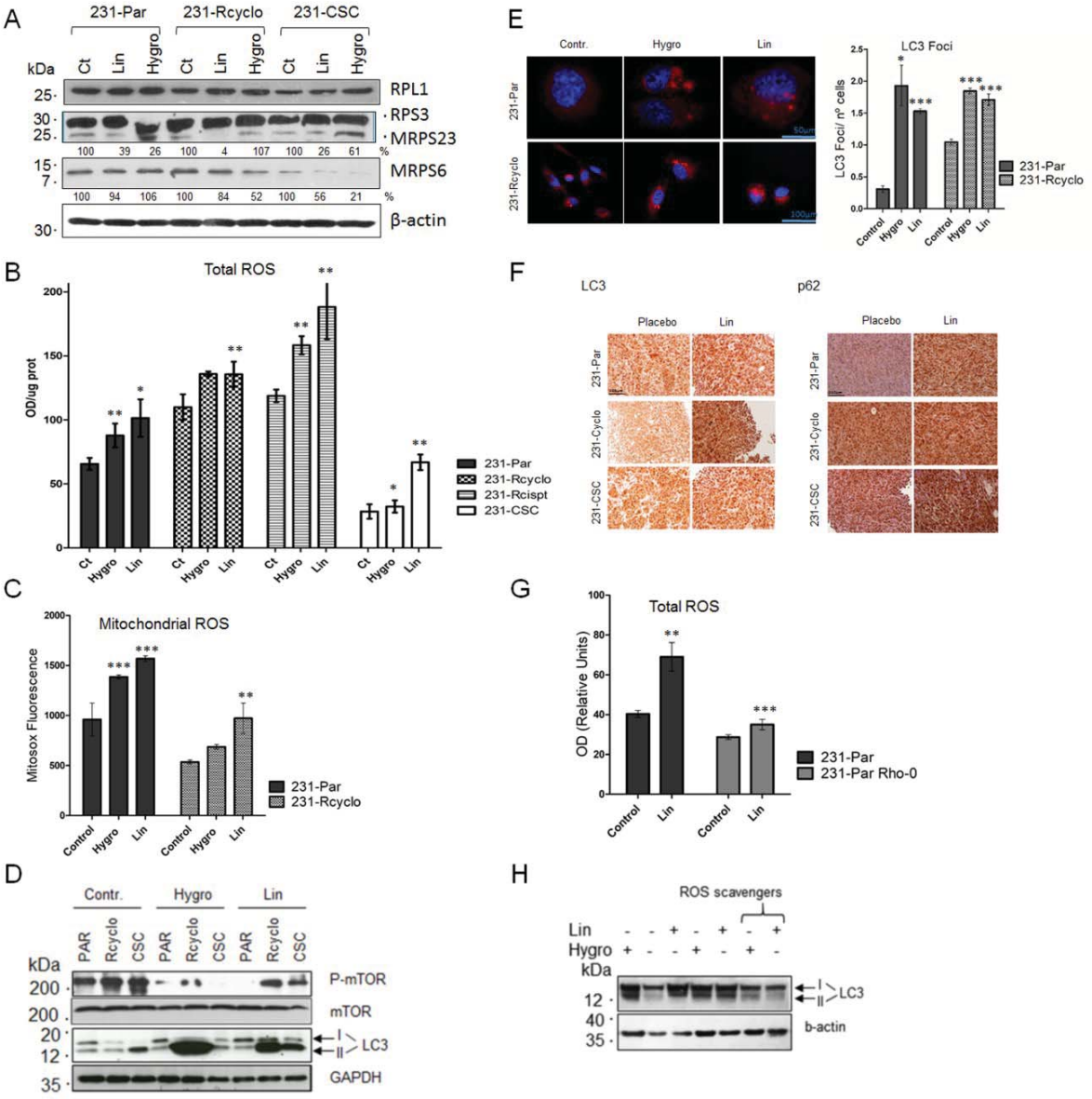

Fig. 5 (page 20)

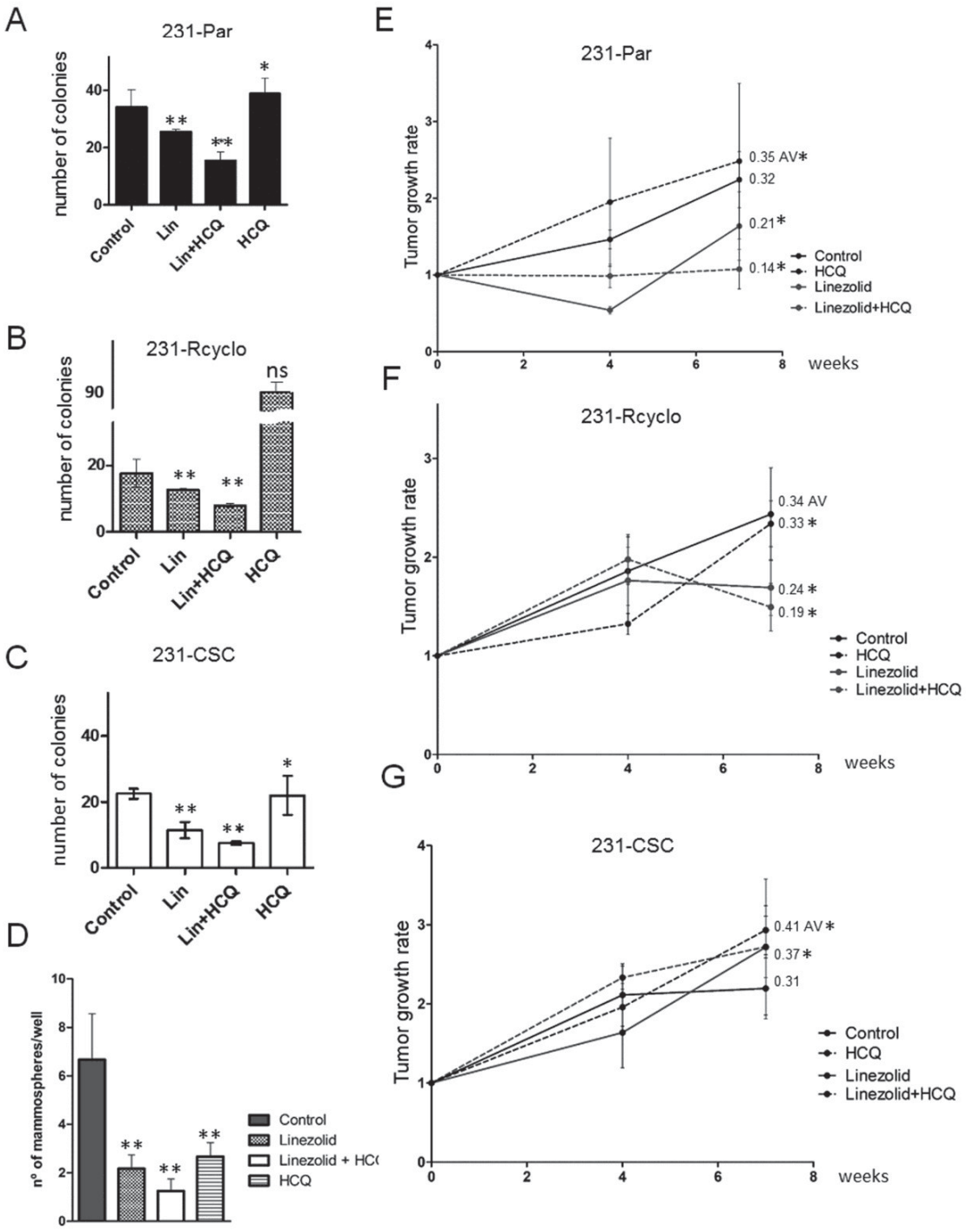

Fig. 6 (page 21)